Z. Phys. C – Particles and Fields 45, 209–222 (1989)

Zeitschrift für Physik C Particles and Fields

Strange baryon production in $e^+ e^-$ annihilation

TASSO Collaboration

W. Braunschweig, R. Gerhards, F.J. Kirschfink, H.-U. Martyn
I. Physikalisches Institut der RWTH Aachen, D-5100 Aachen, Federal Republic of Germany[a]

B. Bock[1], H.M. Fischer, H. Hartmann, J. Hartmann, E. Hilger, A. Jocksch, R. Wedemeyer
Physikalisches Institut der Universität Bonn, D-5300 Bonn, Federal Republic of Germany[a]

B. Foster, A.J. Martin, A.J. Sephton
H.H. Wills Physics Laboratory, University of Bristol, Bristol BS8 1TL, UK[b]

E. Bernardi[2], J. Chwastowski[3], A. Eskreys[3], K. Gather, K. Genser[4], H. Hultschig, P. Joos, H. Kowalski, A. Ladage, B. Löhr, D. Lüke, P. Mättig[5], D. Notz, J.M. Pawlak[4], K.-U. Pösnecker, E. Ros, W. Schütte, D. Trines, R. Walczak[4], G. Wolf
Deutsches Elektronen-Synchrotron, DESY, D-2000 Hamburg, Federal Republic of Germany

H. Kolanoski
Institut für Physik, Universität Dortmund, D-4600 Dortmund, Federal Republic of Germany[a]

T. Kracht[6], J. Krüger, E. Lohrmann, G. Poelz, W. Zeuner[7]
II. Institut für Experimentalphysik der Universität Hamburg, 2000 Hamburg, Federal Republic of Germany[a]

D.M. Binnie, J. Hassard, J. Shulman, D. Su[8]
Department of Physics, Imperial College, London SW7 2AZ, UK[b]

F. Barreiro, A. Leites, L. Hervas, J. del Peso, M. Traseira
Universidad Autonoma de Madrid, Madrid, Spain[c]

C. Balkwill, M.G. Bowler, P.N. Burrows[8], R.J. Cashmore, G.P. Heath, P.N. Ratoff, I.M. Silvester, I.R. Tomalin[9], M.E. Veitch, J.M. Yelton[10]
Department of Nuclear Physics, Oxford University, Oxford OX1 3RH, UK[b]

S.L. Lloyd
Department of Physics, Queen Mary College, London E1 4NS, UK[b]

G.E. Forden[11], J.C. Hart, D.H. Saxon
Rutherford Appleton Laboratory, Chilton, Didcot, Oxon OX11 0QX, UK[b]

S. Brandt, M. Holder, L. Labarga[12]
Fachbereich Physik der Universität-Gesamthochschule Siegen, D-5900 Siegen, Federal Republic of Germany[a]

Y. Eisenberg, U. Karshon, G. Mikenberg, A. Montag, D. Revel, E. Ronat, A. Shapira, N. Wainer, G. Yekutieli
Weizmann Institute, Rehovot 76100, Israel[d]

D. Muller, S. Ritz, D. Strom[13], M. Takashima, Sau Lan Wu, G. Zobernig
Department of Physics, University of Wisconsin, Madison, WI 53706, USA

Received 22 May 1989

[1] Now at Krupp Atlas Elektr. GmbH, Bremen, FRG
[2] Now at Robert Bosch GmbH, Schwieberdingen, FRG
[3] Now at Inst. of Nuclear Physics, Cracow, Poland
[4] Now at Warsaw University, Poland
[5] Now at IPP Canada, Carleton University, Ottawa, Canada
[6] Now at Hasylab, DESY, Hamburg, FRG
[7] Now CERN, CH-1211 Geneva 23, Switzerland
[8] Now at RAL, Chilton, Didcot, Oxon OX11 0QX, UK
[9] Now at Dept. of Physcis, Imperial College, London SW7 2AZ, UK
[10] Now at University of Florida, Gainesville, Florida 32611, USA
[11] Now at SUNY Stony Brook, Stony Brook, NY, USA
[12] Now at SLAC, Stanford, CA, USA
[13] Now at University of Chicago, Chicago, IL, USA

[a] Supported by the Bundesministerium für Forschung und Technologie
[b] Supported by the UK Science and Engineering Research Council
[c] Supported by CAICYT
[d] Supported by the Minerva Gesellschaft für Forschung mbH
[e] Supported by the US Dept. of Energy, contract DE-AC02-76ER00881 and by the U.S. National Science Foundation Grant no. INT-8313994 for travel

Abstract. The production of strange baryons in e^+e^- annihilation has been studied at centre of mass energies of 34.8 GeV and 42.1 GeV, using the TASSO detector at DESY. Inclusive cross-sections have been obtained for Λ^0 and Ξ^- production and an upper limit has been placed upon the production rate of $\Sigma^{*\pm}(1385)$. We measure the Λ^0 multiplicity per event to be $0.218^{+0.011}_{-0.011}\pm0.021$ and $0.256^{+0.030}_{-0.029}\pm0.025$ at $\sqrt{s}=34.8$ and 42.1 GeV respectively. The Ξ^- multiplicity per event is found to be $0.014^{+0.003}_{-0.003}\pm0.004$ at $\sqrt{s}=34.8$ GeV. An investigation has been made of the extent to which Λ^0 are produced in pairs. The Λ^0 cross-section has been studied as a function of event sphericity.

Introduction

Baryon production has been observed in high energy e^+e^- annihilation for some years. By making measurements of the production cross-sections of these particles, as a function of their spin and strangeness, one can hope to throw some light upon the mechanisms through which they are created.

In this paper we present a study of strange baryon production, made using the TASSO detector at the PETRA storage ring at DESY. The analysis used a total of 21891, 8620 and 31176 hadronic events, at mean centre of mass energies, $\sqrt{s}$, of 34.5, 42.1 and 35.0 GeV respectively. The 34.5 GeV data sample was taken with the early TASSO detector configuration [1], whereas the other two data samples were taken after the installation of a vertex detector [2]. These hadronic events were selected using the standard TASSO event cuts, described in [3]. Contamination from non-hadronic background was estimated to be 2.9% in the 34.5 and 42.1 GeV data samples [3], and 1.6% in the 35.0 GeV one [4]. Throughout this paper (with the exception of the section on $\Lambda^0\bar{\Lambda}^0$ correlations), any reference to a particle includes the corresponding antiparticle.

An investigation of Λ^0 production

Λ^0 were found by searching for the decay: $\Lambda^0\to p\pi^-$. All oppositely charged pairs of tracks in each event were considered to be Λ^0 candidates. For each, the higher momentum particle was assumed to be the proton. A series of cuts was then applied in order to reduce the background. The most important of these were that: (1) The distances of closest approach of the two tracks to the e^+e^- beam should each exceed some cut-off. (2) After projection into the plane perpendicular to the beam axis, the angle between the Λ^0 momentum vector and the line joining the interaction point to the Λ^0 vertex should be less than some cut-off. (3) The Λ^0 vertex should not lie within a specified distance of the interaction point. (4) The two track vertex should be of reasonable quality. (5) The $\pi^+\pi^-$ invariant mass of the two tracks should not lie too close to the mass of a K^0. (6) The Λ^0 momentum should exceed some specified cut-off. (7) The $p\pi^-$ invariant mass ot the two tracks should lie within a signal bin of specified width, centred upon the Λ^0 mass.

A more detailed description of these cuts may be found in the Appendix.

When deciding exactly where the cuts should be placed, a novel approach was used. To begin with, all Λ^0 candidates in a set of Monte Carlo events [5] were found, and for each, all the properties to which cuts would be applied were calculated. This information was then stored on disk for easy access. A set of cuts was then found which, when applied to this set of Λ^0 candidates, maximized the signal to noise ratio (i.e. the ratio of the number of real Λ^0 to the number of fake Λ^0 passing the cuts), whilst satisfying the constraint that the efficiency for Λ^0 detection should exceed some specified value. This set of cuts was found using the program MINUIT [6], which is capable of finding the maximum of a function of many variable parameters, subject to any number of constraint equations. In principle, this procedure should have provided the best possible set of Λ^0 selection cuts for given Λ^0 detection efficiency, (although for several reasons this was not quite achieved in practice). A further advantage of this technique is that only Monte Carlo events are used to choose the cuts, and thus one avoids the normal temptation of studying the data in order to find a set of cuts which produces a peak there. It has been shown [7] that when searching for a small signal, the latter procedure is very likely to yield systematically high estimates of particle cross-sections and can even produce completely spurious signals of several standard deviations significance. A far more detailed description of the cut optimization technique may be found in [7].

In order to improve the momentum resolution for real Λ^0, a 3-*D* vertex fit [8] was performed upon each Λ^0 candidate during the course of the Λ^0 selection procedure.

Passing the real data through the MINUIT tuned cuts, with the exception of the $p\pi^-$ invariant mass cut, produced the $p\pi^-$ invariant mass spectra shown in Fig. 1a–c. It is estimated that there are 375, 170 and 932 real Λ^0 over backgrounds of 255, 125 and 986, in the signal bins of these plots, for the 34.5,

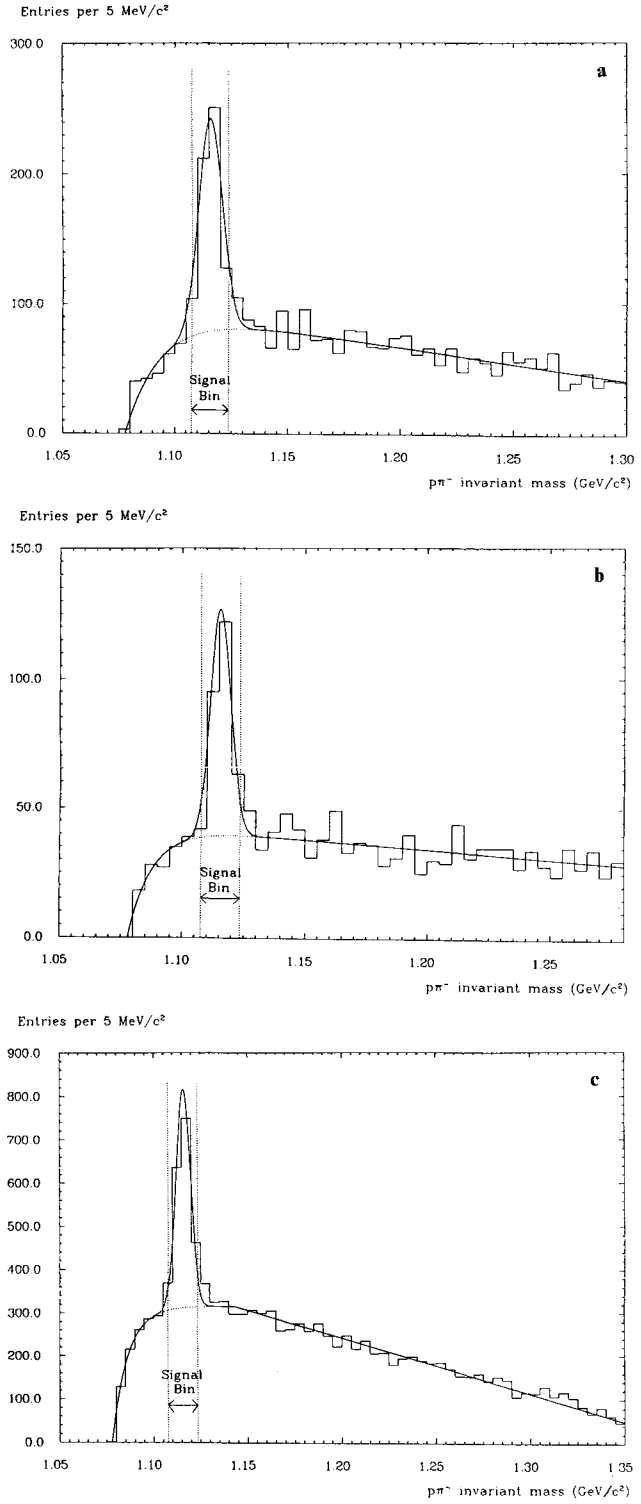

Fig. 1a–c. $p\pi^-$ invariant mass spectra for 34.5, 42.1 and 35.0 GeV data samples respectively

42.1 and 35.0 GeV data samples respectively. Equal numbers of Λ^0 and $\overline{\Lambda^0}$ were found to within statistical errors. These numbers were obtained by making a maximum likelihood fit to each plot, assuming a

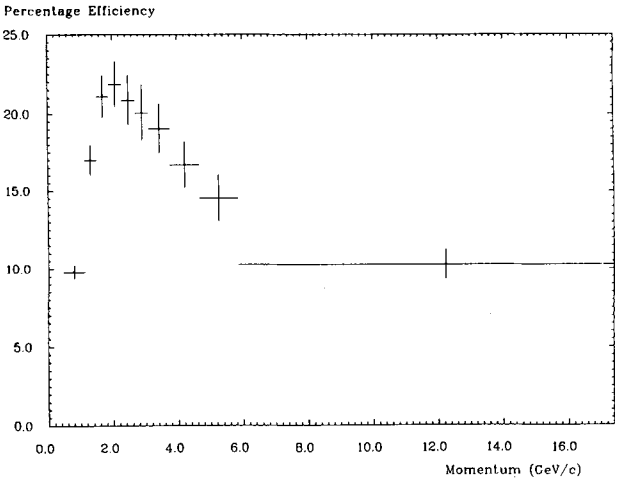

Fig. 2. Λ^0 detection efficiency versus Λ^0 momentum for the 35.0 GeV data sample

Gaussian signal and a smooth background. (In all such fits refered to in this paper, the fit was made over the mass range covered by the curve in the figure, with the exception of the few MeV/c^2 immediately above the threshold). The fits were repeated several times, with various background parametrisations, in order to assess the size of any systematic errors incurred in this step of the analysis. Such errors were found to be present at a level of $\approx \pm 4\%$.

The efficiency for Λ^0 detection was estimated using a new set of Monte Carlo events (generated with a different set of random numbers from those used for the cut optimization). It was found to be 8.6%, 7.9% and 13.6% for the 34.5, 42.1 and 35.0 GeV data samples respectively. Note that the 42.1 and 35.0 GeV data samples benefitted from the presence of the vertex detector, although in the case of the 42.1 GeV data sample, the resultant improvement in the Λ^0 detection efficiency was offset by the effects of the worsening environment inside the detector associated with running at the higher energy. To illustrate the behaviour of the Λ^0 detection efficiency as a function of the Λ^0 momentum, we show this efficiency for the 35.0 GeV data sample in Fig. 2. The efficiency reached its maximum value for Λ^0 momenta of ≈ 2.0 GeV/c, fell away slowly towards higher momenta and was extremely small for momenta below ≈ 0.5 GeV/c.

The size of any systematic errors on these efficiencies, due to uncertainties in the resolution, efficiency and noise levels in the central detector, was assessed by varying these quantities in the Monte Carlo and noting the effect. The contribution from these three sources was found to be $\approx \pm 5\%$, $\approx \pm 6\%$ and $\approx \pm 2\%$ respectively. In addition, because the Λ^0 detection efficiency was quite strongly momentum dependent, we were reliant upon the Monte Carlo cor-

rectly predicting the shape of the Λ^0 differential cross-section with respect to momentum. The size of any systematic error incurred through this reliance was estimated by comparing the predictions of Monte Carlos employing the Lund [9, 10], Webber [11, 12], and various independent jet fragmentation models [13–16]. It was found to be $\approx \pm 4\%$. Included in this error is a contribution of $\approx \pm 1\%$ arising from the need to estimate the unmeasured contribution to the cross-section from low momenta Λ^0 ($p < 0.5$ GeV/c). From the Lund Monte Carlo, we estimate that this low momentum region contains about 4% of all Λ^0 produced. As a final check on systematic errors, the entire analysis was repeated using a few other sets of Λ^0 selection cuts, each set having a different Λ^0 selection efficiency.

It was concluded that $0.218 \,^{+0.011}_{-0.011} \pm 0.021$ and $0.256 \,^{+0.030}_{-0.029} \pm 0.025$ Λ^0 are produced per event at centre of mass energies of 34.8 GeV and 42.1 GeV respectively (having corrected for radiative effects and combined the results obtained from the 34.5 GeV and 35.0 GeV data samples using a simple weighted average). These figures are in excellent agreement with the results obtained from Mark II, TPC and HRS, at $\sqrt{s} = 29$ GeV. These three experiments obtained figures of $0.213 \pm 0.012 \pm 0.018$ [17], $0.197 \pm 0.012 \pm 0.017$ [18] and $0.217 \pm 0.009 \pm 0.022$ [19] respectively. JADE has made a measurement of the Λ^0 cross-section at $\sqrt{s} = 33$ GeV and they obtained a value of 0.234 ± 0.064 Λ^0 per event [20]. The result obtained in the current analysis supersedes the previous TASSO result of $0.31 \pm 0.03 \pm 0.06$ [21] which was based upon a smaller data sample and a different set of Λ^0 selection cuts. We have analysed the 35.0 GeV data sample using the old set of cuts and found results which were in excellent agreement with those given here. It was concluded that the difference between the old and the new TASSO Λ^0 production rates is understood in terms of increased statistics, more realistic fragmentation models and a better understanding of the detector. The Lund* and Webber** Monte Carlos produce 0.220 and 0.262 Λ^0 per event respectively, at $\sqrt{s} = 34.8$ GeV. In passing, it should be noted that both of these fragmentation models can reproduce the measured proton cross-section. The TASSO and TPC collaborations have measured the proton multiplicity per event to be 0.67 ± 0.06 [24] and 0.53 ± 0.07 [25] at $\sqrt{s} = 34$ and 29 GeV respectively. By comparison, the Lund and Webber Monte Carlos

Table 1a–f. The differential cross-sections of the Λ^0 at $\sqrt{s} = 34.8$ GeV

p GeV/c	$\frac{d\sigma}{dp}$ $nb/(\text{GeV/c})$
0.46-1.14	$1.69^{+0.23}_{-0.22} \times 10^{-2}$
1.14-1.51	$1.58^{+0.20}_{-0.20} \times 10^{-2}$
1.51-1.88	$1.47^{+0.18}_{-0.18} \times 10^{-2}$
1.88-2.29	$1.05^{+0.15}_{-0.14} \times 10^{-2}$
2.29-2.70	$1.44^{+0.18}_{-0.17} \times 10^{-2}$
2.70-3.12	$0.98^{+0.16}_{-0.15} \times 10^{-2}$
3.12-3.77	$0.63^{+0.12}_{-0.11} \times 10^{-2}$
3.77-4.66	$0.61^{+0.12}_{-0.11} \times 10^{-2}$
4.66-5.85	$0.45^{+0.08}_{-0.08} \times 10^{-2}$
5.85-17.2	$0.06^{+0.02}_{-0.02} \times 10^{-2}$

$p_\parallel$ GeV/c	$\frac{d\sigma}{dp_\parallel}$ $nb/(\text{GeV/c})$
0.00-0.81	$2.16^{+0.23}_{-0.22} \times 10^{-2}$
0.81-1.22	$1.10^{+0.17}_{-0.16} \times 10^{-2}$
1.22-1.63	$1.36^{+0.17}_{-0.17} \times 10^{-2}$
1.63-2.06	$1.13^{+0.16}_{-0.15} \times 10^{-2}$
2.06-2.49	$1.14^{+0.16}_{-0.16} \times 10^{-2}$
2.49-2.98	$0.92^{+0.14}_{-0.14} \times 10^{-2}$
2.98-3.66	$0.61^{+0.12}_{-0.11} \times 10^{-2}$
3.66-4.56	$0.54^{+0.13}_{-0.11} \times 10^{-2}$
4.56-5.82	$0.46^{+0.08}_{-0.08} \times 10^{-2}$
5.82-17.2	$0.06^{+0.02}_{-0.02} \times 10^{-2}$

$p_{\perp in}$ GeV/c	$\frac{d\sigma}{dp_{\perp in}}$ $nb/(\text{GeV/c})$
0.00-0.068	$7.54^{+1.62}_{-1.67} \times 10^{-2}$
0.068-0.145	$6.30^{+1.48}_{-1.39} \times 10^{-2}$
0.145-0.236	$6.34^{+1.22}_{-1.16} \times 10^{-2}$
0.236-0.331	$8.32^{+1.23}_{-1.18} \times 10^{-2}$
0.331-0.428	$6.56^{+1.09}_{-1.04} \times 10^{-2}$
0.428-0.537	$4.71^{+0.75}_{-0.73} \times 10^{-2}$
0.537-0.691	$3.47^{+0.50}_{-0.48} \times 10^{-2}$
0.691-0.907	$2.91^{+0.35}_{-0.34} \times 10^{-2}$
0.907-1.32	$1.34^{+0.16}_{-0.15} \times 10^{-2}$
1.32-5.40	$0.15^{+0.02}_{-0.02} \times 10^{-2}$

$p_{\perp out}$ GeV/c	$\frac{d\sigma}{dp_{\perp out}}$ $nb/(\text{GeV/c})$
0.00-0.032	$1.54^{+0.26}_{-0.25} \times 10^{-1}$
0.032-0.067	$1.32^{+0.21}_{-0.20} \times 10^{-1}$
0.067-0.107	$1.46^{+0.23}_{-0.22} \times 10^{-1}$
0.107-0.151	$1.52^{+0.22}_{-0.20} \times 10^{-1}$
0.151-0.197	$1.10^{+0.17}_{-0.16} \times 10^{-1}$
0.197-0.251	$0.92^{+0.16}_{-0.15} \times 10^{-1}$
0.251-0.319	$0.93^{+0.15}_{-0.14} \times 10^{-1}$
0.319-0.404	$0.60^{+0.11}_{-0.10} \times 10^{-1}$
0.404-0.545	$0.57^{+0.07}_{-0.07} \times 10^{-1}$
0.545-1.770	$0.08^{+0.01}_{-0.01} \times 10^{-1}$

η	$\frac{d\sigma}{d\eta}$ nb
0.00-0.570	$3.15^{+0.32}_{-0.31} \times 10^{-2}$
0.570-0.817	$2.18^{+0.32}_{-0.31} \times 10^{-2}$
0.817-1.02	$2.33^{+0.33}_{-0.32} \times 10^{-2}$
1.02-1.21	$2.64^{+0.37}_{-0.36} \times 10^{-2}$
1.21-1.39	$2.63^{+0.38}_{-0.38} \times 10^{-2}$
1.39-1.56	$3.13^{+0.44}_{-0.43} \times 10^{-2}$
1.56-1.75	$3.01^{+0.49}_{-0.47} \times 10^{-2}$
1.75-1.97	$1.97^{+0.41}_{-0.39} \times 10^{-2}$
1.97-2.23	$1.84^{+0.37}_{-0.35} \times 10^{-2}$
2.23-3.29	$0.60^{+0.17}_{-0.17} \times 10^{-2}$

x_E	$\frac{s}{\beta} \frac{d\sigma}{dx_E}$ $nb(\text{GeV/c})^2$
0.069-0.092	$11.06^{+1.48}_{-1.42} \times 10^{+2}$
0.092-0.109	$5.64^{+0.70}_{-0.66} \times 10^{+2}$
0.109-0.126	$4.58^{+0.57}_{-0.55} \times 10^{+2}$
0.126-0.148	$2.81^{+0.38}_{-0.37} \times 10^{+2}$
0.148-0.169	$3.65^{+0.47}_{-0.46} \times 10^{+2}$
0.169-0.192	$2.32^{+0.36}_{-0.34} \times 10^{+2}$
0.192-0.229	$1.40^{+0.24}_{-0.23} \times 10^{+2}$
0.229-0.278	$1.42^{+0.26}_{-0.24} \times 10^{+2}$
0.278-0.343	$0.94^{+0.19}_{-0.17} \times 10^{+2}$
0.343-1.000	$0.14^{+0.03}_{-0.03} \times 10^{+2}$

* All comparisons made in this paper between Lund and the data, have been made using JETSET Version 6.2, with most of its parameters being left at their default values as given in [22]. In order to fit the global properties of the data at $\sqrt{s} = 34.8$ GeV, the following parameters were changed (notation as in [22]): PARE(2) $= \Lambda_{\overline{MS}} = 0.52$ GeV, PAR(12) $= 0.42$ GeV/c (the Gaussian P_t of the primary hadrons), PAR(31) $= 0.96$ and PAR(32) $= 0.70$ GeV^{-2} (the a and b parameters in the symmetric Lund fragmentation function). At $\sqrt{s} = 42.1$ GeV, the optimum parameter values were found to be PARE(2) $= 0.99$ GeV, PAR(12) $= 0.40$ GeV/c, PAR(31) $= 1.12$ and PAR(32) $= 0.70$. Good agreement with measured hadron cross-sections was obtained at both energies after changing the parameter PAR(3) $=$ [P(us)/P(ud)]/[P(s)/P(d)] to 0.48. The branching ratio of $\Lambda_c^+ \to \Lambda^0 + X$ was set equal to 23% in accordance with the measurement of [23]

** All comparisons made in this paper between the Webber model [11, 12] and the data have been made using version 4.2 with B. Webber's recommended parameter values: $\Lambda_{LL} = 0.35$ GeV, maximum cluster mass $= 3.75$ GeV/c^2, gluon virtual mass cutoff $= 0.75$ GeV/c^2, and u, d, s, c and b quark masses of 0.004, 0.008, 0.15, 1.80 and 5.2 GeV/c^2 respectively

Table 2a–f. The differential cross-sections of the Λ^0 at $\sqrt{s}$ = 42.1 GeV

p GeV/c	$\frac{d\sigma}{dp}$ $nb/(\text{GeV/c})$
0.61-1.29	$1.36^{+0.38}_{-0.35} \times 10^{-2}$
1.29-1.88	$1.53^{+0.32}_{-0.29} \times 10^{-2}$
1.88-2.68	$0.80^{+0.20}_{-0.19} \times 10^{-2}$
2.68-4.14	$0.52^{+0.12}_{-0.11} \times 10^{-2}$
4.14-17.5	$0.10^{+0.03}_{-0.03} \times 10^{-2}$

$p_{\parallel}$ GeV/c	$\frac{d\sigma}{dp_{\parallel}}$ $nb/(\text{GeV/c})$
0.00-0.995	$1.69^{+0.39}_{-0.36} \times 10^{-2}$
0.995-1.66	$1.31^{+0.30}_{-0.28} \times 10^{-2}$
1.66-2.48	$0.67^{+0.20}_{-0.18} \times 10^{-2}$
2.48-3.97	$0.60^{+0.13}_{-0.12} \times 10^{-2}$
3.97-17.5	$0.08^{+0.03}_{-0.03} \times 10^{-2}$

$p_{\perp in}$ GeV/c	$\frac{d\sigma}{dp_{\perp in}}$ $nb/(\text{GeV/c})$
0.00-0.152	$8.32^{+2.32}_{-2.16} \times 10^{-2}$
0.152-0.337	$4.63^{+1.82}_{-1.68} \times 10^{-2}$
0.337-0.583	$2.73^{+0.96}_{-0.88} \times 10^{-2}$
0.583-0.976	$2.47^{+0.53}_{-0.50} \times 10^{-2}$
0.976-4.86	$0.32^{+0.06}_{-0.05} \times 10^{-2}$

$p_{\perp out}$ GeV/c	$\frac{d\sigma}{dp_{\perp out}}$ $nb/(\text{GeV/c})$
0.00-0.080	$1.28^{+0.35}_{-0.33} \times 10^{-1}$
0.032-0.165	$1.40^{+0.32}_{-0.30} \times 10^{-1}$
0.067-0.273	$1.11^{+0.28}_{-0.18} \times 10^{-1}$
0.107-0.451	$0.25^{+0.12}_{-0.11} \times 10^{-1}$
0.151-1.910	$0.10^{+0.02}_{-0.02} \times 10^{-1}$

η	$\frac{d\sigma}{d\eta}$ nb
0.00-0.686	$2.59^{+0.53}_{-0.49} \times 10^{-2}$
0.686-1.04	$2.13^{+0.49}_{-0.47} \times 10^{-2}$
1.04-1.38	$1.94^{+0.53}_{-0.50} \times 10^{-2}$
1.38-1.79	$2.04^{+0.50}_{-0.48} \times 10^{-2}$
1.79-3.43	$0.65^{+0.25}_{-0.23} \times 10^{-2}$

x_E	$\frac{s}{\beta}\frac{d\sigma}{dx_E}$ $nb(\text{GeV/c})^2$
0.060-0.081	$12.1^{+3.2}_{-3.0} \times 10^{+2}$
0.081-0.106	$8.3^{+1.8}_{-1.7} \times 10^{+2}$
0.106-0.138	$3.8^{+0.9}_{-0.9} \times 10^{+2}$
0.138-0.204	$2.6^{+0.6}_{-0.6} \times 10^{+2}$
0.204-0.811	$0.4^{+0.1}_{-0.1} \times 10^{+2}$

produce 0.68 and 0.54 protons per event at $\sqrt{s}$ = 34.8 GeV.

Differential cross-sections with respect to momentum (p), rapidity (η) (calculated with respect to the sphericity axis) and momentum components parallel to the sphericity axis ($p_{\parallel}$) and perpendicular to this axis in ($p_{\perp \text{in}}$) and out ($p_{\perp \text{out}}$) of the event plane were obtained. The scaled cross section $(\frac{s}{\beta}\frac{d\sigma}{dx_E})$ was also calculated (where β is the Λ^0 velocity and x_E is the Λ^0 energy, expressed as a fraction of the beam energy). These are given in Tables 1a–f and 2a–f, where an overall systematic error of $\approx \pm 9\%$ due to the systematic effects described above is not included. We have also not included the systematic error of $\pm 5\%$ which was present due to our uncertainty in R. In calculating the differential cross-sections, we used $R = 4.01 \pm 0.03 \pm 0.20$, in accordance with out earlier measurement [3]. (Here R denotes the ratio of the total hadronic cross-section to the lowest order QED $\mu^+\mu^-$ cross-section). Figures 3a–c and 4a–c show $\frac{d\sigma}{dp}$, $\frac{d\sigma}{dp_{\perp \text{in}}}$ and $\frac{d\sigma}{dp_{\perp \text{out}}}$ for the 34.8 and 42.1 GeV Λ^0 samples respectively, along with the predictions of the Lund Monte Carlo. It can be seen that Lund reproduces the measured differential cross-sections very well. (Note that the differential cross-sections obtained from the data have been averaged over the

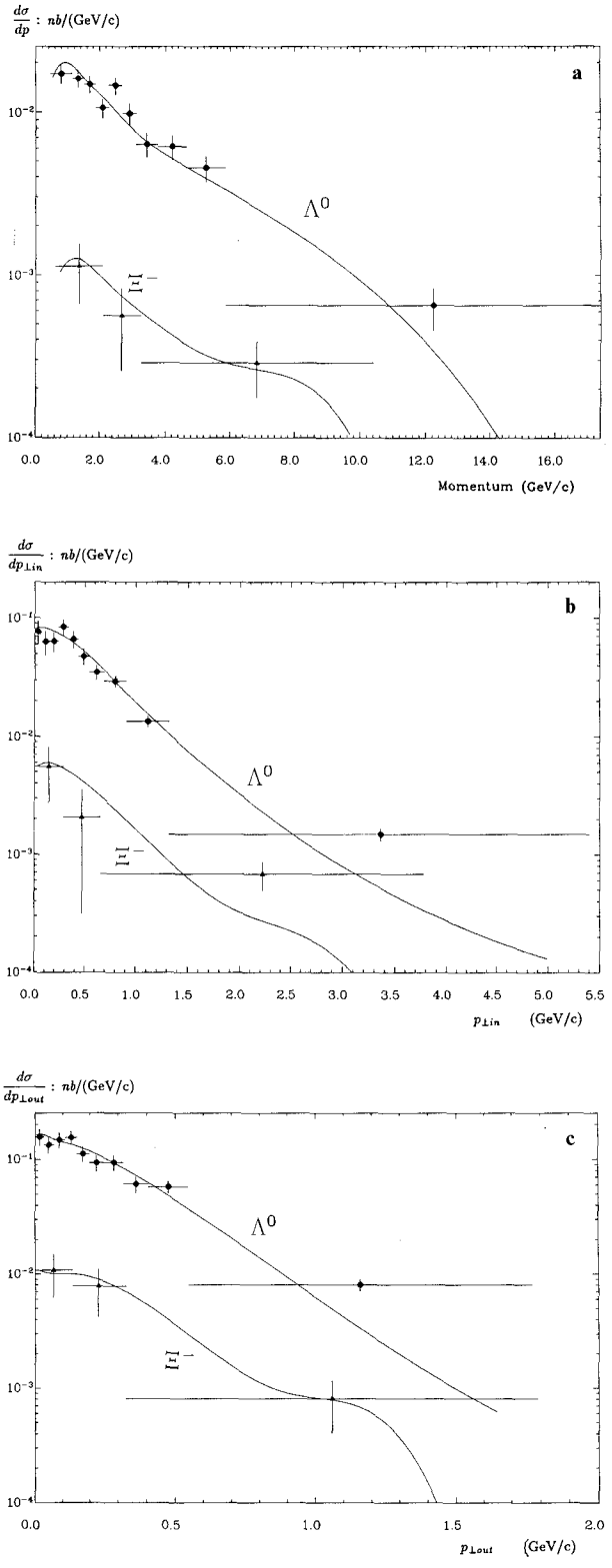

Fig. 3a. $\frac{d\sigma}{dp}$ for Λ^0 and Ξ^- production at $\sqrt{s} = 34.8$ GeV. **b** $\frac{d\sigma}{dp_{\perp \text{in}}}$ for Λ^0 and Ξ^- production at $\sqrt{s} = 34.8$ GeV. **c** $\frac{d\sigma}{dp_{\perp \text{out}}}$ for Λ^0 and Σ^- production at $\sqrt{s} = 34.8$ GeV. The curves show the Lund predictions

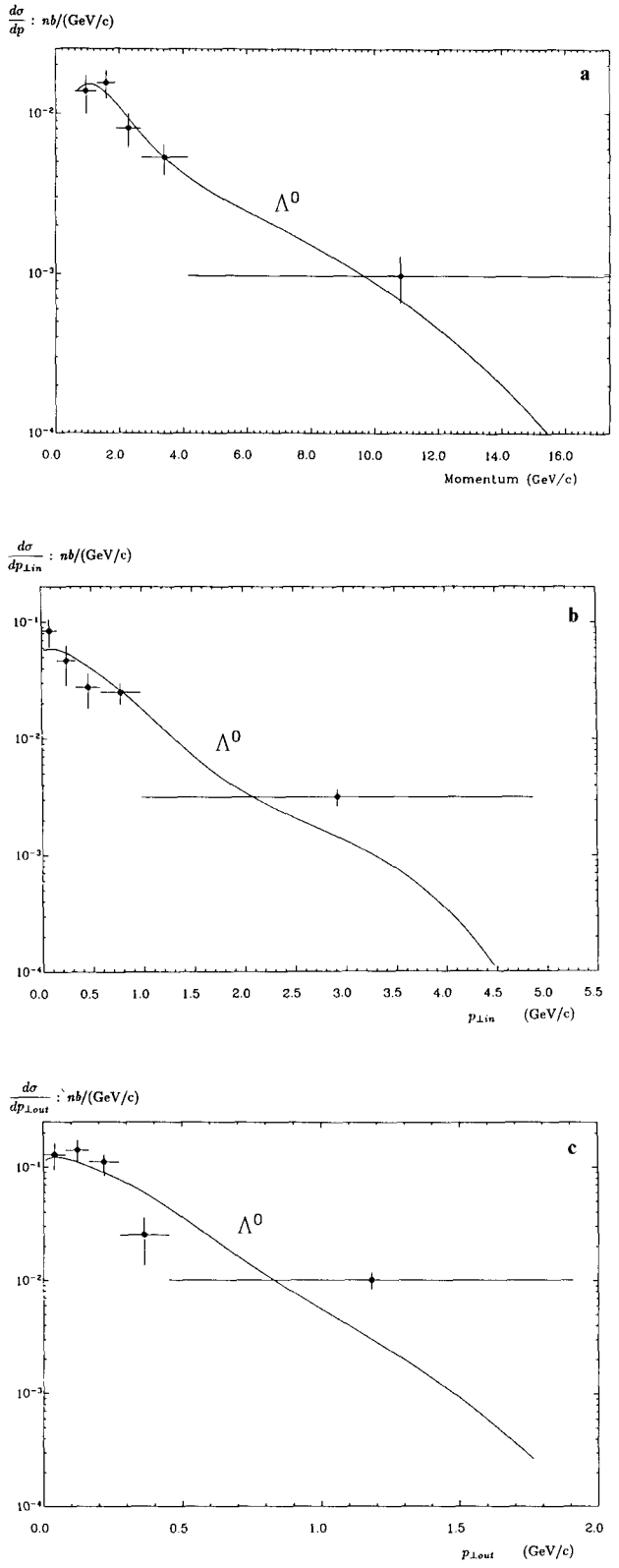

Fig. 4a. $\frac{d\sigma}{dp}$ for Λ^0 production at $\sqrt{s}=42.1$ GeV. **b** $\frac{d\sigma}{dp_{\perp in}}$ for Λ^0 production at $\sqrt{s}=42.1$ GeV. **c** $\frac{d\sigma}{dp_{\perp out}}$ for Λ^0 production at $\sqrt{s}=42.1$ GeV. The curves show the Lund predictions

given momentum ranges, whereas the curves representing the Lund predictions have not.)

A study was then made of the extent to which Λ^0 are produced in pairs. Combining the 34.5 GeV and 35.0 GeV data samples, we found in total 27.8 real $\Lambda^0\bar{\Lambda}^0$ pairs over a background of 17.6, and 2.8 real $\Lambda^0\Lambda^0+\bar{\Lambda}^0\bar{\Lambda}^0$ pairs over a background of 16.9. We estimate that $0.052\,^{+0.013}_{-0.012}\pm0.010$ $\Lambda^0\bar{\Lambda}^0$ pairs are produced per event at $\sqrt{s}=34.8$ GeV. This number compares well with the results of TPC and HRS, which obtained figures of $0.042\pm0.017\pm0.014$ [18] and $0.054\pm0.014\pm0.012$ [19] respectively, at $\sqrt{s}=29$ GeV. For comparison, Lund predicts a number of 0.045. The result obtained from the data implies that $47.7\,^{+11.7}_{-10.8}\pm4.7\%$ of all Λ^0 are produced in such pairs, which is over four times the proportion one would expect in the absence of any correlations ($11.0\pm0.6\pm1.1\%$).

Dividing each event into two hemispheres, separated by the plane perpendicular to the sphericity axis, it was found that there was a $71\,^{+11}_{-11}\%$ chance of both particles in a $\Lambda^0\bar{\Lambda}^0$ pair going into the same hemisphere. The data thus provides some evidence for local conservation of baryon number and/or strangeness during fragmentation. The Lund prediction for this number is 69%.

In addition, it was estimated that $0.0052\,^{+0.0087}_{-0.0052}\pm0.0010$ $\Lambda^0\Lambda^0+\bar{\Lambda}^0\bar{\Lambda}^0$ pairs are produced per event (i.e. $4.8\,^{+7.8}_{-4.8}\pm0.5\%$ of all Λ^0 are produced in such pairs). This is consistent with what would be expected in the absence of any correlations. The Lund prediction for this number is 0.0082.

Finally, Λ^0 production was investigated as a function of event sphericity (S). The results of this analysis are presented in Table 3a and b and plotted along with the Lund predictions in Fig. 5a–d. It is apparent that the number of Λ^0 produced per event (n_{Λ^0}), does increase quite fast with increasing event sphericity and there is some indication that it does so faster than the total charged multiplicity does. Lund underestimates the size of the increase. As high sphericity events arise mainly as a result of hard gluon bremsstrahlung, this result suggests that Λ^0 are produced more prolifically in gluon jets than in quark jets. However, $b\bar{b}$ events also have fairly high sphericities, so one can not draw any firm conclusions. A similar effect has been observed in Λ^0 production by Mark II [17] and in proton production by TPC [26]. CLEO [27] and ARGUS [28] have established that baryons

Table 3a, b. Λ^0 production as a function of event sphericity at $\sqrt{s}$ = 34.8 GeV (**a**) and $\sqrt{s}$ = 42.1 GeV (**b**)

Event Sphericity	n_{Λ^0}	n_{charge}	$\frac{n_{\Lambda^0}}{n_{charge}}$
0.000-0.022	$0.174^{+0.022}_{-0.021}$	9.6	$0.0180^{+0.0023}_{-0.0022}$
0.022-0.037	$0.119^{+0.024}_{-0.023}$	11.6	$0.0102^{+0.0021}_{-0.0020}$
0.037-0.053	$0.212^{+0.028}_{-0.027}$	12.7	$0.0167^{+0.0023}_{-0.0021}$
0.053-0.072	$0.172^{+0.025}_{-0.024}$	13.2	$0.0131^{+0.0019}_{-0.0019}$
0.072-0.091	$0.159^{+0.032}_{-0.031}$	13.9	$0.0115^{+0.0023}_{-0.0022}$
0.091-0.120	$0.200^{+0.031}_{-0.028}$	14.3	$0.0140^{+0.0021}_{-0.0020}$
0.120-0.163	$0.237^{+0.032}_{-0.028}$	14.7	$0.0160^{+0.0021}_{-0.0020}$
0.163-0.232	$0.263^{+0.032}_{-0.030}$	15.3	$0.0172^{+0.0021}_{-0.0019}$
0.232-0.347	$0.265^{+0.035}_{-0.033}$	15.7	$0.0169^{+0.0022}_{-0.0021}$
0.347-0.842	$0.293^{+0.030}_{-0.028}$	16.4	$0.0178^{+0.0018}_{-0.0017}$

Event Sphericity	n_{Λ^0}	n_{charge}	$\frac{n_{\Lambda^0}}{n_{charge}}$
0.000-0.035	$0.185^{+0.048}_{-0.045}$	11.8	$0.0157^{+0.0041}_{-0.0038}$
0.035-0.071	$0.160^{+0.052}_{-0.048}$	14.6	$0.0110^{+0.0035}_{-0.0033}$
0.071-0.134	$0.231^{+0.069}_{-0.064}$	16.2	$0.0143^{+0.0043}_{-0.0039}$
0.134-0.245	$0.404^{+0.085}_{-0.079}$	17.1	$0.0237^{+0.0050}_{-0.0046}$
0.245-0.729	$0.446^{+0.080}_{-0.075}$	17.8	$0.0250^{+0.0045}_{-0.0042}$

are produced at an enhanced rate in the 3 gluon decay of the Υ, relative to the neighbouring continuum.

An investigation of Ξ^- production

Ξ^- were found by searching for the decay chain: $\Xi^- \to \Lambda^0 \pi^-$ followed by $\Lambda^0 \to p\pi^-$. All oppositely charged pairs of tracks were considered to be Λ^0 candidates; the track with the higher momentum was assumed to be the proton, the other track the pion. A third track was then searched for with the same charge as the pion. It was assumed to be the pion which had come directly from the Ξ^- decay. In order to reject fake Ξ^- a number of cuts were then applied, of which the most important were: (1) The distances of closest approach of all three tracks to the e^+e^- beam should each exceed some cut-off. (2) After projection into the plane perpendicular to the beam axis, the angle between the Ξ^- momentum vector and the line joining the interaction point to the Ξ^- vertex should be less than some cut-off. (3) The Ξ^- vertex should not lie within a specified distance of the inter-

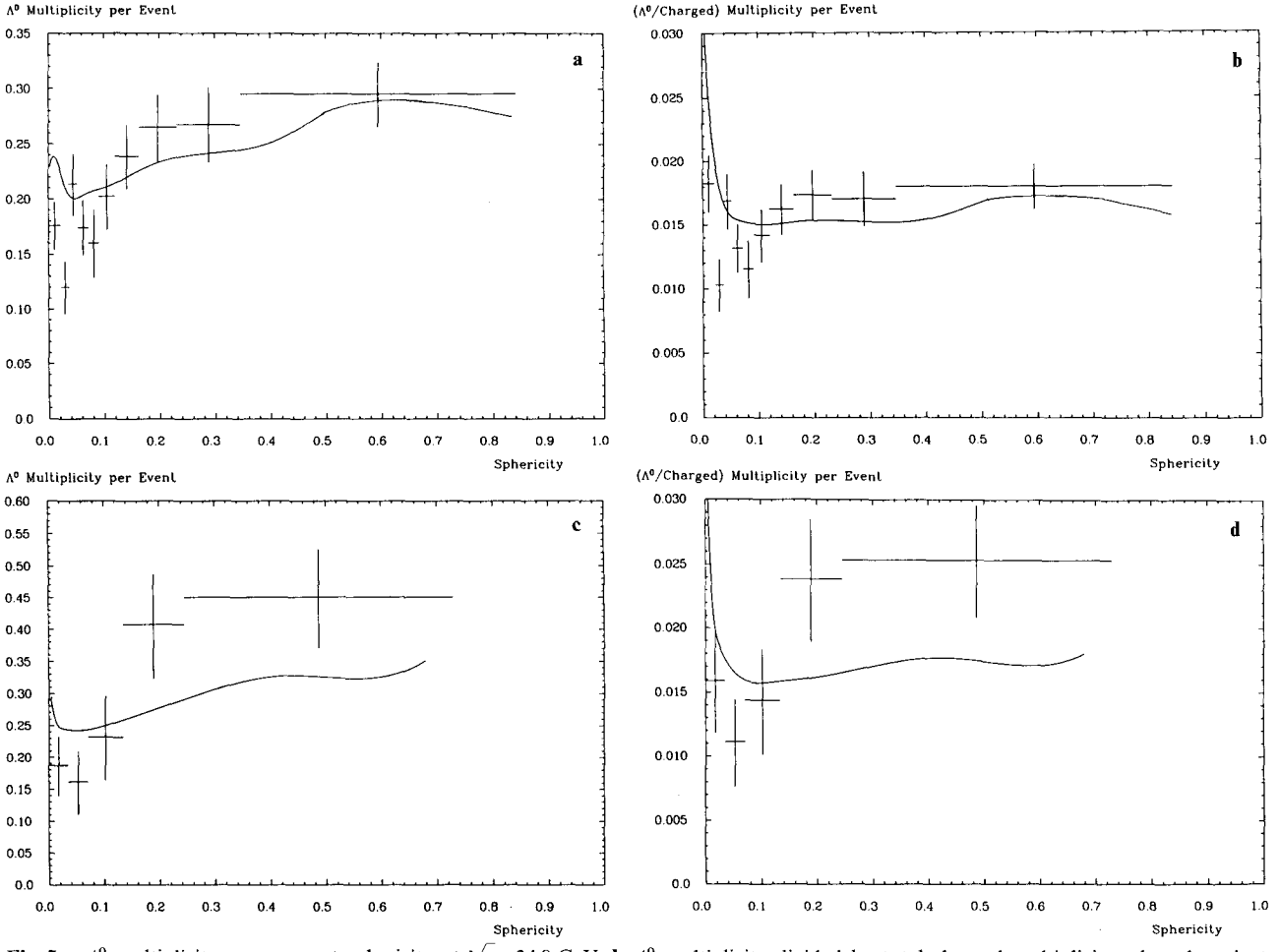

Fig. 5a. Λ^0 multiplicity versus event sphericity at $\sqrt{s}$ = 34.8 GeV. **b** Λ^0 multiplicity divided by total charged multiplicity, plotted against event sphericity at $\sqrt{s}$ = 34.8 GeV. **c** Λ^0 multiplicity versus event sphericity at $\sqrt{s}$ = 42.1 GeV. **d** Λ^0 multiplicity divided by total charged multiplicity, plotted against event sphericity at $\sqrt{s}$ = 42.1 GeV. The curves show the Lund predictions

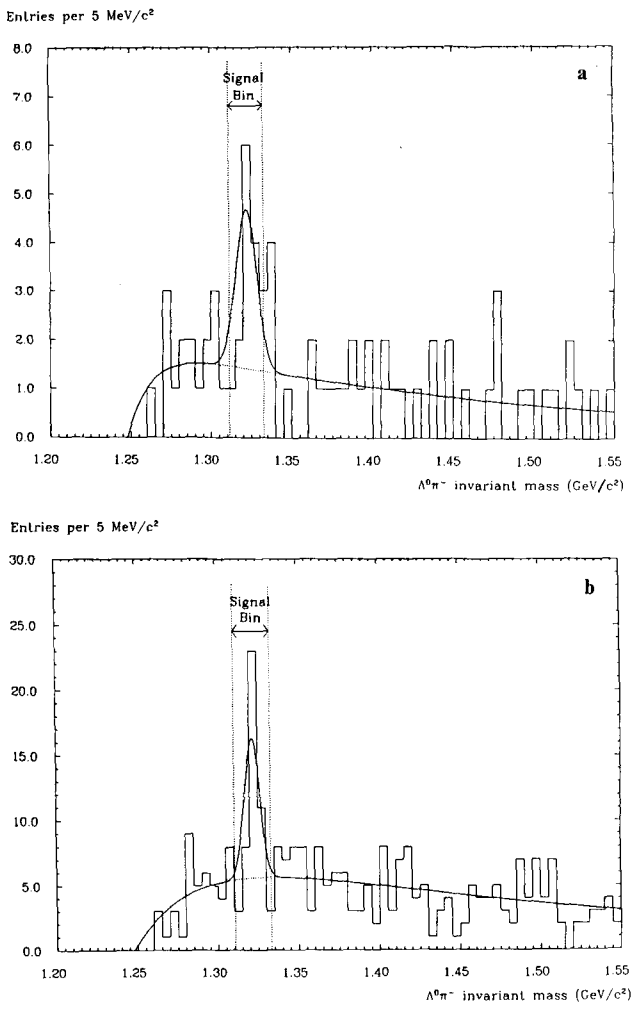

Fig. 6a, b. $\Lambda^0\pi^-$ invariant mass spectra for 34.5 and 35.0 GeV data samples respectively

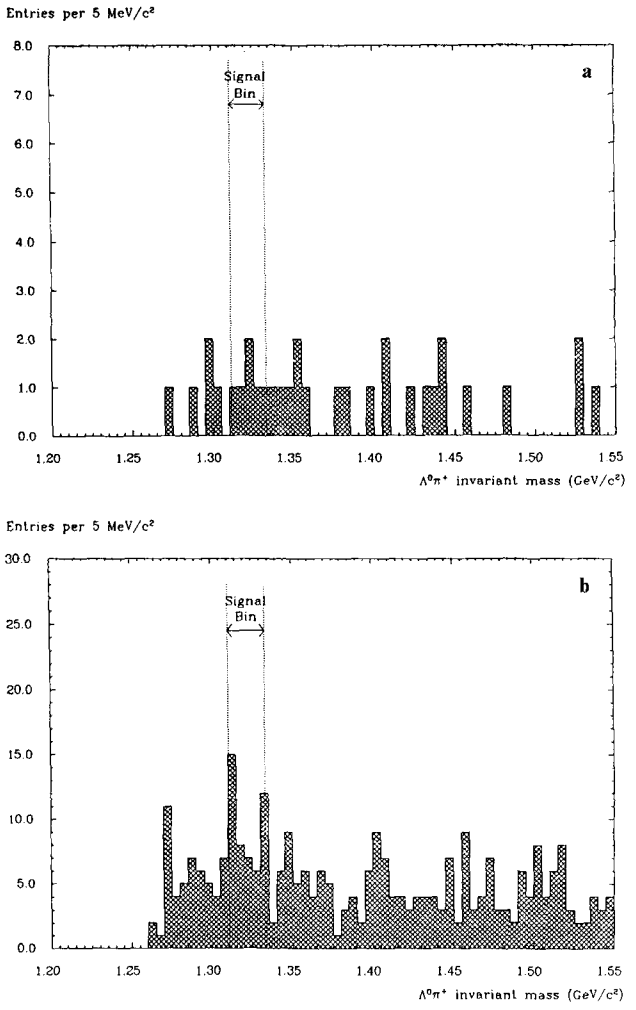

Fig. 7a, b. $\Lambda^0\pi^+$ invariant mass spectra for 34.5 and 35.0 GeV data samples respectively

action point or within a specified distance from the Λ^0 vertex. (4) The tracks intersecting at the Λ^0 and Ξ^- decay points should form vertices of acceptable quality. (5) The Ξ^- momentum should exceed some specified cut-off. (6) The $p\pi^-$ invariant mass of the Λ^0 candidate should lie close to the true Λ^0 mass. (7) The $\Lambda^0\pi^-$ invariant mass of the Ξ^- candidate should lie within a signal bin of specified width, centred upon the true Ξ^- mass.

A more detailed description of these cuts may be found in the Appendix.

The cuts were optimised using MINUIT (as in the Λ^0 analysis) so as to maximize the signal to noise ratio obtained.

The momentum resolution for real Ξ^- was significantly improved by making a 3-*D* vertex fit [8] to the Λ^0 candidate, and then refitting all three tracks subject to two additional constraints. These were that the $p\pi^-$ invariant mass of the Λ^0 candidate should be precisely equal to the true Λ^0 mass, and that the projected flight path of the Λ^0 should intersect (in 3-*D*) the flight path of the pion which had come directly from the Ξ^- decay. These track-refits were carried out during the course of the Ξ^- selection procedure.

Passing the data through these cuts, with the exception of that applied to the $\Lambda^0\pi^-$ invariant mass, produced the $\Lambda^0\pi^-$ invariant mass spectra shown in Fig. 6a and b. For comparison, the wrong sign, $\Lambda^0\pi^+$ mass spectra are given in Fig. 7a and b. The 42.1 GeV data sample was not used, being too small to make its analysis worthwhile. By making a maximum likelihood fit to each of these spectra, it was estimated that there were 10.1 and 24.8 real Ξ^- over backgrounds of 7.5 and 25.3, in the signal bins of these two plots, for the 34.5 and 35.0 GeV data samples respectively. Surprisingly the two data samples contained in total 25.4 Ξ^- and only 9.5 $\bar{\Xi}^+$. The absorption cross-section for anti-baryons is larger than that

for baryons, but this would only lead one to expect a charge asymmetry of approximately 5%. We therefore assume that the observed asymmetry is just a statistical fluctuation. However, it is curious that an analysis by Mark II found 29 Ξ^- and only 12 $\bar{\Xi}^+$ [30] and that one by HRS found 9.6 Ξ^- and only 5.8 $\bar{\Xi}^+$ [31].

Using a set of Monte Carlo events, the efficiency for Ξ^- detection was estimated to be 3.8% and 6.0% for the 34.5 and 35.0 GeV data samples respectively. The efficiency was extremely small for Ξ^- momenta of less than ≈ 0.7 GeV/c and we were forced to rely upon the Lund and Webber fragmentation models to predict the fraction of Ξ^- being produced in this region. (In doing this, it was encouraging to note that the two models gave almost identical predictions for the shape of the Ξ^- momentum spectrum and that the Lund model described well the shape of the Λ^0 spectrum – as mentioned earlier in this paper). Systematic errors on the efficiencies were estimated using similar methods to those employed in the Λ^0 analysis. Again, a check on these was made by trying a few different sets of Ξ^- selection cuts.

When calculating the total cross-section for Ξ^- production, the results obtained from the 34.5 and 35.0 GeV data samples were combined. As the statistics involved were small, this was not done using a simple weighted average, but rather by multiplying together the two likelihood functions which had been obtained from the fits to the two $p\pi^-\pi^-$ invariant mass spectra. In this manner, it was concluded that at $\sqrt{s}=34.8$ GeV, a total of $0.012^{+0.003}_{-0.003}\pm 0.003$ Ξ^- are produced per event. This result lies below the old TASSO figure of $0.026\pm0.008\pm0.009$ [29], which was obtained using a different set of Ξ^- selection cuts and a much smaller data sample. Inverstigations showed that the difference between these two results arose from a number of sources: most notably from statistical fluctuations, the use of more up to date fragmentation models and a better simulation of the behaviour of the detector. As a check, the 34.5 and 35.0 GeV data samples were reanalysed using the original TASSO cuts [29]. This yielded a result of $0.016\pm0.005\pm0.004$ Ξ^- per event (having combined the two data samples), in good agreement with that obtained using the new analysis procedure. For the final TASSO number, we averaged the two results (remembering that they are not statistically independent) and concluded that $0.014^{+0.003}_{-0.003}\pm 0.004$ Ξ^- are produced per event (having corrected for radiative effects).

This result agrees to within errors with the results of Mark II and HRS, which found $0.017\pm0.004\pm0.004$ [30] and $0.016\pm0.004\pm0.004$ [31] Ξ^- per event respectively, at $\sqrt{s}=29$ GeV. For comparison, the Lund and Webber Monte Carlos produce 0.017 and 0.039 Ξ^- per event respectively, at $\sqrt{s}=34.8$ GeV.

Table 4a–f. The differential cross-sections of the Ξ^- at $\sqrt{s}=34.8$ GeV

p GeV/c	$\frac{d\sigma}{dp}$ $nb/(\mathrm{GeV/c})$
0.62-2.10	$11.3^{+4.8}_{-4.3}\times10^{-4}$
2.10-3.27	$5.8^{+3.0}_{-2.6}\times10^{-4}$
3.27-10.4	$2.9^{+1.3}_{-1.0}\times10^{-4}$

$p_{\parallel}$ GeV/c	$\frac{d\sigma}{dp_{\parallel}}$ $nb/(\mathrm{GeV/c})$
0.00-1.82	$8.9^{+4.0}_{-3.6}\times10^{-4}$
1.82-3.08	$7.0^{+3.1}_{-2.8}\times10^{-4}$
3.08-10.4	$2.4^{+1.0}_{-0.9}\times10^{-4}$

$p_{\perp in}$ GeV/c	$\frac{d\sigma}{dp_{\perp in}}$ $nb/(\mathrm{GeV/c})$
0.00-0.285	$5.6^{+2.9}_{-2.5}\times10^{-3}$
0.285-0.656	$2.1^{+1.8}_{-1.5}\times10^{-3}$
0.656-3.78	$0.7^{+0.2}_{-0.2}\times10^{-3}$

$p_{\perp out}$ GeV/c	$\frac{d\sigma}{dp_{\perp out}}$ $nb/(\mathrm{GeV/c})$
0.00-0.134	$10.8^{+4.6}_{-4.1}\times10^{-3}$
0.134-0.327	$7.8^{+3.6}_{-3.1}\times10^{-3}$
0.327-1.79	$0.8^{+0.4}_{-0.4}\times10^{-3}$

η	$\frac{d\sigma}{d\eta}$ nb
0.00-0.985	$1.3^{+0.6}_{-0.6}\times10^{-3}$
0.985-1.46	$2.9^{+1.0}_{-0.9}\times10^{-3}$
1.46-2.67	$1.3^{+0.6}_{-0.6}\times10^{-3}$

x_E	$\frac{s}{\beta}\frac{d\sigma}{dx_E}$ $nb(\mathrm{GeV})^2$
0.084-0.144	$5.4^{+2.1}_{-1.9}\times10^{+1}$
0.144-0.206	$1.1^{+0.8}_{-0.6}\times10^{+1}$
0.206-0.606	$0.7^{+0.3}_{-0.2}\times10^{+1}$

Differential cross-sections for Ξ^- production are given in Table 4a–f, where overall systematic errors of $\pm20\%$ and $\pm5\%$, due to imperfections in the Monte Carlo and uncertainties in the value of R respectively, are not included. $\frac{d\sigma}{dp}$, $\frac{d\sigma}{dp_{\perp in}}$ and $\frac{d\sigma}{dp_{\perp out}}$ together with the Lund predictions are plotted in Fig. 3a–c.

A search for $\Sigma^{*\pm}$ (1385) production

$\Sigma^{*\pm}$ were searched for by looking for the decay chain: $\Sigma^{*\pm}\to\Lambda^0\pi^\pm$ followed by $\Lambda^0\to p\pi^-$. The Λ^0 and $\pi^\pm$ resulting from a $\Sigma^{*\pm}$ decay are invariably produced extremely close to the e^+e^- interaction point. This meant that the Λ^0 could be searched for using an almost identical selection procedure to that employed in the Λ^0 analysis. When looking for the $\pi^\pm$, the most important cuts applied were that: (1) Its distance of closest approach to the e^+e^- beam should be less than some cut-off. (2) The reconstructed $\Sigma^{*\pm}$ vertex should lie within some specified distance of the interaction point. Unfortunately, because most of the particles in a typical hadronic event are produced near to the interaction point, these two cuts allowed through a lot of background. A detailed list of the cuts applied may be found in the Appendix.

The optimum values for these cuts were again

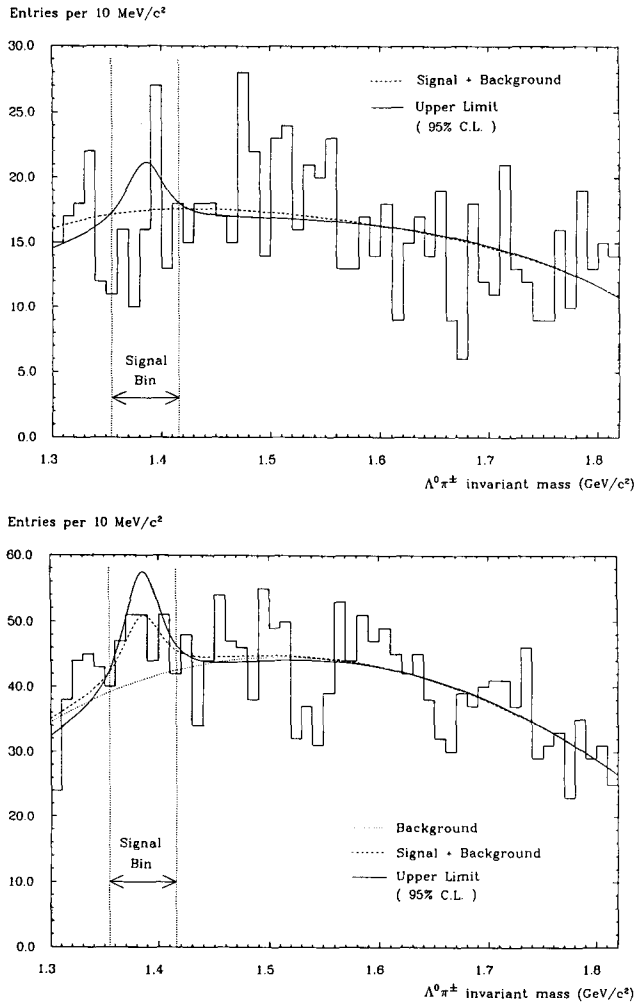

Fig. 8a, b. $\Lambda^0\pi^\pm$ invariant mass spectra for 34.5 and 35.0 GeV data samples respectively

found by allowing MINUIT to process information obtained from a set of Monte Carlo events.

During the course of the $\Sigma^{*\pm}$ selection procedure, all three tracks in each $\Sigma^{*\pm}$ candidate were refitted, as was done in the Ξ^- analysis, so as to improve the momentum resolution.

Passing the data though these cuts produced the $p\pi^\pm\pi^-$ invariant mass spectra shown in Fig. 8a and b. If $\Sigma^{*\pm}$ were produced in abundance, then one would see a peak centred upon a mass of 1.385 GeV/c^2, and of full-width (at half height) $\approx$40.0 MeV/c^2. No significant peak is observed.

From the Monte Carlo events, the efficiency for $\Sigma^{*\pm}$ selection was estimated to be 2.2% and 3.8% for the 34.5 and 35.0 GeV data samples respectively. The efficiency was extremely small for $\Sigma^{*\pm}$ momenta of less than $\approx$0.8 GeV/c. As in the Ξ^- analysis, the systematic error on these two efficiencies was estimated to be of the order of $\pm$23%. Once again, a few different sets of $\Sigma^{*\pm}$ selection cuts were tried out when performing the analysis, as a double check on these systematic errors.

A maximum likelihood fit was then made to both mass spectra simultaneously (combining the information which they each contained). The likelihood function, $L(\sigma, U_1, U_2 \ldots U_6)$, used in this fit, was simply set equal to the product of the likelihood functions of the two separate mass spectra. Here, σ was the $\Sigma^{*\pm}$ cross-section and U_1 to U_6 were parameters used to describe the background curves.

Because the background in the $\Sigma^{*\pm}$ analysis was significant, we tried out several different parametrisations of it when performing this fit. This gave us some idea of the systematic errors which the fit introduced. The signal was fitted with the convolution of a Gaussian (representing the experimental resolution) with an s-wave Breit-Wigner. (Although the $\Sigma^{*\pm}$ actually decays via a p-wave, an s-wave Breit-Wigner has been found to describe it better [32]). The fits indicated that a $\Sigma^{*\pm}$ peak was present at somewhere between the 1.5 and 2.8 standard deviation level; the exact significance depending on which set of $\Sigma^{*\pm}$ selection cuts were used and on which parametrisations were employed when fitting the mass spectra.

When trying to place an upper limit on the $\Sigma^{*\pm}$ cross-section, one is faced with the problem that the term "upper limit" is not uniquely defined (see for example [33–35]). In order to assess the size of this problem, it was decided to calculate the upper limit, using two of the most commonly used definitions of the term, and then to compare the results. These were;

i) To define the 95% confidence level upper limit on σ, to be that value of σ for which $\log_e(L)$ is 1.92 below its maximum value ($\log_e(L)$ being maximised with respect to the other parameters (U_1 to U_6 whilst σ is varied).

ii) To assume that the likelihood function, when evaluated at $(\sigma, U_1 \ldots U_6)$, is proportional to the likelihood of these parameters taking those particular values. The probability distribution of σ can then be found by integrating $L(\sigma, U_1 \ldots U_6)$ over the uninteresting parameters (U_1 to U_6) and then normalizing it (so that its integral over all allowed values of σ is equal to unity). From this probability distribution the upper limit on σ can be calculated.

Some justification for both of these definitions is given in [36].

In practice, it was found that both definitions gave very similar (but not identical) results. Using the second definition, it was possible to take into account the systematic uncertainties on the $\Sigma^{*\pm}$ detection efficiency by convoluting a Gaussian of appropriate width with the probability distribution of σ.

In this manner, it was concluded at a confidence

level of 95%, that fever than 0.053 $\Sigma^{*\pm}$ are produced per event at $\sqrt{s}=34.8$ GeV (having corrected for radiative effects). For comparison, the Lund and Webber Monte Carlos produce 0.042 and 0.084 $\Sigma^{*\pm}$ per event respectively, at this energy.

HRS have observed a $\Sigma^{*\pm}$ signal at $\sqrt{s}=29$ GeV and quote a result of $0.033\pm0.006\pm0.005$ [37] $\Sigma^{+\pm}$ per event. The previous TASSO result was an upper limit at 95% confidence level, of 0.09 $\Sigma^{*\pm}$ per event [38].

ARGUS have also measured the $\Sigma^{*\pm}$ cross-section [28], with significantly better statistics. They deduced that at $\sqrt{s}\approx10$ GeV (continuum), the ratio of $\Sigma^{*\pm}$ to Λ^0 production is $0.116\pm0.016\pm0.020$. If one assumes that this ratio is the same at $\sqrt{s}=34.8$ GeV, then one predicts that $0.024\pm0.003\pm0.004$ $\Sigma^{*\pm}$ per event would be produced at this centre of mass energy. This is consistent with the results given in this section and indeed would help to explain the presence of the small peak observed in this analysis.

Conclusions

We have measured the Λ^0 multiplicity per event to be $0.218^{+0.011}_{-0.011}\pm0.021$ and $0.256^{+0.030}_{-0.029}\pm0.025$ at $\sqrt{s}=34.8$ and 42.1 GeV respectively. The Ξ^- multiplicity per event is found to be $0.014^{+0.003}_{-0.003}\pm0.004$ at $\sqrt{s}=34.8$ GeV. Differential cross-sections for Λ^0 and Ξ^- production have been obtained. All these results are found to be well described by the Lund fragmentation model. The Webber model produces too many strange baryons. Note that small variations in the maximum allowed cluster mass in the Webber model, can easily alter the baryon production rates by a factor of ten or so. However, if one were to reduce the strange baryon production rate in this manner, then one would obtain too few protons.

We find that $0.052^{+0.013}_{-0.012}\pm0.012$ $\Lambda^0\bar{\Lambda}^0$ pairs and $0.0052^{+0.0087}_{-0.0052}\pm0.012$ $\Lambda^0\Lambda^0+\bar{\Lambda}^0\bar{\Lambda}^0$ pairs are produced per event at $\sqrt{s}=34.8$ GeV. In 71^{+11}_{-11}% of the $\Lambda^0\bar{\Lambda}^0$ pairs, both particles go into the same hemisphere (taken with respect to the sphericity axis). This provides some evidence for local conservation of baryon number and is in excellent agreement with the Lund model predictions.

We observe that the Λ^0 multiplicity rises as a function of event sphericity. The total charged multiplicity also increases, but apparently not quite as fast. Lund underestimates the size of the increase.

An upper limit has been placed upon the number of $\Sigma^{*\pm}$ (1385) produced per event, of 0.053 at 95% confidence level. This is consistent with the cross-section measurement by HRS.

Appendix

In this appendix is given a list of the cuts used to find Λ^0, Ξ^- and $\Sigma^{*\pm}$. All the cuts given were optimized using MINUIT as explained in the main text. Although a large number of cuts were used, this should not cause the reader concern. There are two reasons for this. Firstly, the cuts were optimized by studying Monte Carlo events as opposed to studying the data, and as explained in the main text, this eliminates a major source of systematic errors associated with choosing one's cuts. Secondly, it became apparent after performing the MINUIT cut optimization, that the optimal values of some cuts were so loose as to make them almost irrelevant. They could easily have been left out of the analysis without significantly altering the final results.

Notation

In this appendix, frequent reference will be made to the TASSO coordinate system. In this system, the z-axis runs parallel to the beam, and the r-ϕ plane lies perpendicular to it. The origin of the coordinate system lies at the centre of the detector.

P_t denotes the momentum component of a track in the r-ϕ plane. The quantity $D_{0\,\mathrm{beam}}$ is the distance of closest approach of a track to the e^+e^- interaction point, after projection into the r-ϕ plane. Here the e^+e^- interaction point was taken to be at the centre of the beam spot, as determined from tracks accumulated during several hours of running [39]. The measured beam size ($\approx330\times90$ μm^2) was sufficiently small as to be unimportant to the analysis presented here.

The tracks used in the analyses

The 34.5 GeV data sample was taken with the early configuration of the TASSO detector [1], in which the central detector consisted of a central proportional chamber (CPC) surrounded by a large drift chamber (DC). Tracks were reconstructed from the hits in these two chambers using a track-finder known as MILL [40].

The 42.1 and 35.0 GeV data samples were taken after the installation of a vertex detector (VXD) [2]. To make use of the VXD, we employed a track-finder known as PASS 5 [41]. This extrapolated each MILL track into the VXD and attempted to associate VXD hits with it. In order to ensure that tracks were relia-

bly reconstructed in the VXD, PASS 5 tracks were only retained if they had hits assigned to them in at least four out of the eight layers of the VXD. For the purposes of the current analysis, if PASS 5 failed to extend a particular MILL track into the VXD, then we just used the MILL track for the analysis instead. In order to check systematic errors, the Λ^0 analysis of the 35.0 GeV data sample was repeated using an independent track finder known as FELIX [42]. This also searched for tracks in all three chambers of the central detector, but unlike PASS 5, it made no use of MILL tracks.

All tracks used in the analyses were required to pass a few standard TASSO quality cuts.

i.e. They were required to have $P_t > 0.1$ GeV/c; $|\cos\theta| < 0.87$ and $|Z_0| < 20.0$ cm

Here, θ is the angle which the track's momentum vector makes with the beam axis and Z_0 is the z-coordinate of the track at its distance of closest approach to the beam.

The Λ^0 selection cuts

In this section, the cuts used to identify Λ^0 are given. Those cuts used to measure the Λ^0 cross-section will be given in round brackets: ( ), whereas those used whilst searching for Ξ^- and $\Sigma^{*\pm}$ will be given in the brackets: [ ] and { } respectively. Because the conditions were different at each energy studied, the cuts were tuned separately for each of the three data samples. Inside each of the brackets, the cuts used for the 34.5, 42.1 and 35.0 GeV data samples will be given in that order. Note however that the 42.1 GeV data sample was only used in the Λ^0 analysis. Also note that the cuts described in paragraphs 1) and p) were not applied when searching for Ξ^- or $\Sigma^{*\pm}$. When searching for Ξ^-, neither were cuts described in paragraphs i), j) and k). The cuts used were as follows;

a) The pion $D_{0\,\mathrm{beam}}$ should be greater than (0.34, 0.17, 0.24) [0.33, 0.20] {0.39, 0.30} cm
b) The proton $D_{0\,\mathrm{beam}}$ should be greater than (0.00, 0.08, 0.03) [0.13, 0.05] {0.00, 0.13} cm
c) The pion $D_{0\,\mathrm{beam}} \times P_t \times \beta$ should be greater than (0.15, 0.06, 0.05) [0.23, 0.04] {0.14, 0.04} cm·GeV/c
d) The proton $D_{0\,\mathrm{beam}} \times P_t \times \beta$ should be greater than (0.28, 0.06, 0.06) [0.16, 0.04] {0.30, 0.07} cm·GeV/c

Cuts a) to d) are designed to eliminate the large number of particles which were produced close to the interaction point. Cuts c) and d) were developed after noting that the contribution to these particle's $D_{0\,\mathrm{beam}}$ due to scattering is proportional to $1/(P_t \times \beta)$. As most of the particles in each event were pions, the particle velocity β was calculated from the momentum assuming pion mass.

e) There should be no more than (2, 4, 4) [3, 4] {2, 5} hits assigned to either the proton or the pion, in the central detector, before the Λ^0 vertex.

In order to ensure that the two tracks almost intersected in 3-dimensions, the following pair of cuts was applied;

f) After projection into the r-ϕ plane, the flight paths of the proton and the pion should be no further than (0.1, 0.3, 0.2) [1.0, 1.0] {1.0, 1.0} cm apart at their point of closest approach.
g) At the point at which the tracks intersect in the r-ϕ plane, (or their point of closest approach if they don't intersect), the proton and pion tracks should differ in their z-coordinates by no more than (4.1, 10.1, 15.4) [17.0, 17.0] {17.0, 17.0} cm.
h) In order to improve the momentum resolution for real Λ^0, a 3-D vertex fit [7] was then performed upon each Λ^0 candidate. The confidence level associated with the increase in χ^2 which occurred as a result of forcing the two tracks to intersect was then calculated. To check the vertex quality it was required that this exceed (0.0, 2.3×10^{-7}, 0.0) [4.9×10^{-9}, 0.0] {6.2×10^{-12}, 0.0}.

A further improvement in momentum resolution was achieved by making a mass dependent correction to each particle's momentum, in order to take into account the energy loss which it suffered in passing through the beam-pipe etc.

i) The Λ^0 vertex was required to be at least (1.7, 1.5, 1.0) {4.2, 1.2} cm away from the beam spot in the r-ϕ plane and at least (4.8, 1.6, 2.1) {8.3, 1.9} cm away from it in 3-dimensions.
j) The Λ^0 vertex was required to lie within a momentum dependent minimum and maximum distance from the beam spot, corresponding to probabilities of (0.14, 0.08, 0.09) {0.09, 0.14} % and (1.00, 1.00, 1.00) {1.00, 0.99} % of a Λ^0 decaying before reaching that distance.
k) The Λ^0 momentum vector was required to point back towards the interaction point to within (3.3, 2.8, 3.3) {1.4, 2.5} degrees in the r-ϕ plane and to within (15.0, 80.0, 115.0) {15.0, 60.0} degrees in 3-dimensions.
l) All Λ^0 candidates were required to have a momentum of at least (0.61, 0.61, 0.46) GeV/c.
m) The angle θ^* between the proton momentum vector and the Λ^0 flight path, as measured in the rest frame of the Λ^0, was required to satisfy $|\cos\theta^*| \leqq$(0.98, 0.97, 0.98) [0.95, 0.96] {0.90, 0.93}. This cut favours particles with large $D_{0\,\mathrm{beam}}$ and situations in which one of the two particles being considered has far larger momentum than the other (as is normally the case for real Λ^0)
n) If both tracks are assumed to be pions, then the

$\pi^+\pi^-$ invariant mass should differ from the K^0 mass by the least (1.1, 1.5, 0.5) [0.0, 0.0] {13.0, 9.0} MeV/c^2.
o) If both tracks are assumed to be electrons, then the e^+e^- invariant mass should be greater than (50.0, 70.0, 65.0) [80.0, 65.0] {20.0, 90.0} MeV/c^2.
p) Λ^0 candidates were required to have a $p\pi^-$ invariant mass such that they lay inside a signal bin, which was centred upon the true Λ^0 mass and had a half width of (8.1, 8.0, 7.9) MeV/c^2.

The Ξ^- selection cuts

In this section the cuts used to identify Ξ^- are given. Throughout the section, the symbol π_1^- will be used to denote the π^- which came directly from the Ξ^- decay, whereas the symbol π_2^- will be used to denote the π^- which came from the Λ^0 decay. Having obtained a sample of Λ^0 as described in the previous section, the following additional cuts were applied;

a) The $D_{0\,\mathrm{beam}}$ of the π_1^- should be greater than [0.07, 0.10] cm.
b) $D_{0\,\mathrm{beam}} \times P_t \times \beta$ of the π_1^- should be greater than [0.00, 0.03] cm. GeV/c
c) There should be no more than 2 hits assigned to π_1^- before the Ξ^- vertex.
d) After projection into the r-ϕ plane, the flight paths of the Λ^0 and the π_1^- should be no further than 1.0 cm apart at their point of closest approach.
e) At the point at which they intersect in the r-ϕ plane, (or their point of closest approach if they don't intersect), the Λ^0 and π_1^- tracks should differ in their z-coordinates by no more than 25.0 cm.
f) A significant improvement in momentum resolution for real Ξ^- was then obtained by refitting all three tracks subject to the following two constraints;
i) That the $p\pi_2^-$ invariant mass should be precisely equal to the true Λ^0 mass.
ii) That the projected flight path of the Λ^0 should intersect the flight path of π_1^-. After this refit, the following additional cuts were applied;

g) The Λ^0 vertex was required to be at least [0.13, 0.10] cm away from the Ξ^- vertex in the r-ϕ plane and at least [0.13, 0.10] cm away from it in 3-dimensions. Similarly, the Ξ^- vertex should be at least [0.8, 0.4] cm away from the interaction point in r-ϕ and at least [3.2, 1.9] cm away from it in 3-dimensions.
h) The Ξ^- momentum vector was required to point back towards the beam spot to within [3.2, 4.7] degrees in r-ϕ and [40.0, 145.0] degrees in 3-dimensions.
i) The Ξ^- vertex was required to lie closer to the interaction point that the Λ^0 one (although a 2.0 cm tolerance was allowed on this).
j) All Ξ^- candidates were required to have a momentum of at least [0.79, 0.60] GeV/c.
k) The Λ^0 vertex was required to lie within a momentum dependent minimum and maximum distance from the Ξ^- vertex, corresponding to probabilities of [0.00, 0.01] % and [0.99, 0.98] % of a Λ^0 decaying before reaching that distance. Similarly, the Ξ^- should lie within a momentum dependent distance of the beam spot, with corresponding probabilities of [0.13, 0.08] % and [0.99, 0.99] % respectively.
l) The decay angle $\theta^*_{\Lambda^0}$ of the Λ^0 in the rest frame of the Ξ^-, taken with respect to the Ξ^- flight path, should satisfy $|\cos\theta^*_{\Lambda^0}| \leqq [0.97, 0.99]$
m) Ξ^- candidates were required to have a $\Lambda^0\pi_1^-$ invariant mass such that they lay inside a signal bin, which was centred upon the true Ξ^- mass and had a half width of [13.3, 11.3] MeV/c^2.

The $\Sigma^{*\pm}$ selection cuts

In this section, the cuts used to identify $\Sigma^{*\pm}$ are given. The Λ^0 were searched for as described earlier in this Appendix. The following additional cuts were then applied;

a) The $D_{0\,\mathrm{beam}}$ of the $\pi^\pm$ should be less than {0.58, 0.19} cm
b) $D_{0\,\mathrm{beam}} \times P_t \times \beta$ for the $\pi^\pm$ should be less than {0.75, 0.20} cm. GeV/c
c) The $p\pi_2^-$ invariant mass was required to lie in the region from {8.1, 7.8} MeV/c^2 below the true Λ^0 mass to {8.7, 8.4} MeV/c^2 above it.
d) In order to improve the momentum resolution of those tracks which were the result of a genuine $\Sigma^{*\pm}$ decay, all three tracks were then subject to a constrained refit, as was done in the Ξ^- analysis.
After this refit, the following additional cuts were applied;
d) The $\Sigma^{*\pm}$ vertex was required to be less than {9.6, 2.6} cm away from the beam spot in r-ϕ and less than {9.6, 3.8} cm away from it in 3-dimensions.
e) All $\Sigma^{*\pm}$ candidates were required to have a momentum of at least {0.88, 1.14} GeV/c.
f) The decay angle $\theta^*_{\Lambda^0}$ of the Λ^0 in the rest frame of the $\Sigma^{*\pm}$, taken with respect to the $\Sigma^{*\pm}$ flight path, was required to satisfy $\cos\theta^*_{\Lambda^0} \geqq \{-0.98, -0.99\}$

This cut is slightly different to the analogous ones employed in the Λ^0, and Ξ^- analyses, in that it does not eliminate those $\Sigma^{*\pm}$ candidates with $\cos\theta^*_{\Lambda^0} \approx +1$. This change means that the cut still disfavours those $\Sigma^{*\pm}$ candidates in which the Λ^0 and $\pi^\pm$ have similar momenta (which is frequently the case for fake $\Sigma^{*\pm}$, but not often true for real ones). However, it will not eliminate those $\pi^\pm$ tracks with small $D_{0\,\mathrm{beam}}$.

g) $\Sigma^{*\pm}$ candidates were required to have a $\Lambda^0\pi^\pm$ invariant mass such that they lay inside a signal bin,

which was centred upon the true $\Sigma^{*\pm}$ mass and had a half width of $\{30.6, 30.5\}$ MeV/c^2.

Acknowledgements. We gratefully acknowledge the support of the DESY directorate, the PETRA machine group for high luminosity running and the staff of the DESY and RAL computer centres. Those of us from outside DESY wish to thank the DESY directorate for the hospitality extended to us.

References

1. TASSO Coll. R. Brandelik et al.: Phys. Lett. 83B (1979) 261
2. D.M. Binnie et al., Nucl. Instrum Methods. 228 (1985) 267
3. TASSO Coll. R. Brandelik et al.: Phys. Lett. 113B (1982) 499; TASSO Coll. M. Althoff et al.: Phys. Lett. 138B (1984) 441
4. TASSO Coll. W. Braunschweig et al.: to be published (1988)
5. All Monte Carlo events used were generated with detector simulation being performed by the SIMPLE program of B. Foster and S. Lloyd (unpublished)
6. F. James, M. Roos: Comp. Phys. Commun. 10 (1976) 343; The MINUIT writeup is also available from the CERN computer library
7. I.R. Tomalin: D. Phil. Thesis Oxford University (1988); Rutherford Report RL-HEP/T/069
8. D.H. Saxon: Nucl. Instrum. Methods A234 (1985) 258
9. T. Sjöstrand: Comp. Phys. Commun. 27 (1982) 243
10. T. Sjöstrand: Comp. Phys. Commun. 28 (1983) 229
11. G. Marchesini, B.R. Webber: Nucl. Phys. B238 (1984) 1
12. B.R. Webber: Nucl. Phys. B238 (1984) 492
13. P. Hoyer et al.: Nucl. Phys. B161 (1979) 349
14. A. Ali, E. Pietarinen, G. Kramer, J. Willrodt: Phys. Lett. 93B (1980) 155
15. T. Meyer, Z. Phys. C – Particles and Fields 12 (1982) 77
16. K. Fabricius, G. Kramer, G. Schierholz, I. Schmidt: Phys. Lett. 97B (1981) 431
17. Mark II Collaboration, C. de la Vaissiere et al.: Phys. Rev. Lett. 54 (1985) 2071
18. TPC Collaboration, H. Aihara et al.: Phys. Rev. Lett. 54 (1985) 274
19. HRS Coll. P. Baringer et al.: Phys. Rev. Lett. 56 (1986) 1346
20. JADE Coll. W. Bartel et al.: Phys. Lett. 104B (1981) 325
21. TASSO Coll. M. Althoff et al.: Z. Phys. C – Particles and Fields 27 (1985) 27
22. T. Sjöstrand: Comp. Phys. Commun. 39 (1986) 347
23. SLAC Hybrid Facility Photon Coll. K. Abe et al.: Phys. Rev. D33 (1986) 1
24. TASSO Coll. W. Braunschweig et al., DESY 88-164 (1988)
25. TPC Coll. H. Aihara et al.: LBL 23737-1988 (1988)
26. TPC Coll. H. Aihara et al.: Phys. Rev. Lett. 53 (1984) 130
27. CLEO Coll. S. Behrends et al.: Phys. Rev. D31 (1985) 2161
28. ARGUS Coll. H. Albrecht et al.: DESY 87-141 (1987)
29. TASSO Coll. M. Althoff et al.: Phys. Lett. 130B (1983) 340
30. Mark II Coll. S.R. Klein et al.: Phys. Rev. Lett. 58 (1987) 644
31. HRS Coll. S. Abachi et al.: Phys. Rev. Lett. 58 (1987) 2627
32. Particle Data Group, Review of Particle Properties: Phys. Lett. 170B (1986) 315
33. A.G. Frodeson, O. Skjeggestad, H. Tøfte: Probability and statistics in particle physics, pp. 24–29 (Universitetsforlaget, 1979)
34. M.G. Kendall, A. Stuart: The advanced theory of statistics 3rd Edit. Vol. 2, pp. 159–165. Griffin 1973
35. H. Jeffries: The theory of probability 3rd Edit. Oxford: Oxford University Press 1961
36. A.G. Frodeson, O. Skjeggestad, H. Tøfte: Probability and statistics in particle physics pp. 28–29, pp. 229–236 (Universitetsforlaget, 1979)
37. HRS Coll. S. Abachi et al.: Phys. Rev. Lett. 58 (1987) 2627
38. TASSO Coll. M. Althoff et al.: Z. Phys. C – Particles and Fields 26 (1984) 181
39. TASSO Coll. W. Braunschweig et al.: Z. Phys. C – Particles and Fields 39 (1988) 331
40. D. Cassel, H. Kowalski: Nucl. Instrum. Methods 185 (1981) 235
41. W. Schütte: Thesis, University of Hamburg, Interner Bericht, DESY F1-84/03
42. A.J. Campbell: Ph. D. Thesis, University of London (1983); Rutherford Report RL-HEP/T/117